Results in Physics 24 (2021) 104086

Contents lists available at ScienceDirect

Results in Physics

journal homepage: www.elsevier.com/locate/rinp

Numerical investigations on the cascaded high harmonic and quasi-supercontinuum generations in epsilon-near-zero aluminum-doped zinc oxide nanolayers

Jiaye Wu [a], Ze Tao Xie [a], H.Y. Fu [b], Qian Li [a,*]

[a] School of Electronic and Computer Engineering, Peking University, Shenzhen 518055, China
[b] Tsinghua-Berkeley Shenzhen Institute (TBSI), Tsinghua University, Shenzhen 518055, China

ARTICLE INFO

Keywords:
Epsilon-near-zero
Cascaded harmonic generation
Aluminum-doped zinc oxide
Transparent conducting oxide
Quasi-supercontinuum

ABSTRACT

The cascaded high harmonic generations (HHG) and quasi-supercontinuum (quasi-SC) generations by epsilon-near-zero (ENZ) aluminum-doped zinc oxide (AZO) nanolayers are demonstrated numerically. Due to AZO's high second- and third-order nonlinear responses, the ENZ AZO nanolayer is capable of generating high harmonic waves up to the 15th order under the excitation of a pico- or femtosecond laser source. The conversion efficiencies for the third, fifth, and seventh harmonic generations, estimated by the ratio of the spectral peak power, are in theory, comparable with the experimental results of ENZ indium tin oxide and indium-doped cadmium oxide. By broadening HHG peaks, the quasi-SC generation in nanolayers with different thickness is discussed. The results of this work might be useful in designing nanoscale multiwavelength light sources.

Introduction

Epsilon-near-zero (ENZ) materials, as a category of near-zero-index (NZI) materials, are at the frontiers in the fields of plasmonic optics, nonlinear optics, and nanophotonics [1–5]. At the vicinity of the ENZ wavelength where the real part of its complex permittivity slowly vanishes, the electromagnetic (EM) wave can tunnel through the structure [6] with a nearly unchanged phase [7], amplified electric field intensity [8], confined by novel ENZ modes [9], and experience slow-light effect [10] and enhanced nonlinearity [11].

Transparent conducting oxides (TCOs), a type of commonly used materials in modern microelectronic industries, are inexpensive candidates for ENZ realization in the near-infrared region. Their ultrahigh optical nonlinear response [12] enables the theoretical and experimental discoveries of complex self-interaction patterns of ultrashort pulses [13,14], second-harmonic generations (SHGs) [15,16], third-harmonic generations (THGs) [16–18], and high harmonic generations (HHGs) [19,20] up to the 9th order [19], as well as applications such as electro- and all-optical switching [21–23].

As for HHGs, up to 15th harmonic generation has been achieved in non-ENZ setups [24,25], reaching the ultraviolet (UV) regime. The benefits of using ENZ material for harmonic generation are that the NZI condition enables the use of a weaker source thanks to field enhancement and efficient frequency conversion [26]. However, for ENZ materials, there are few theoretical and numerical studies on SHG, THG, and HHG. In this case, numerical simulations would allow new possibilities to be explored and discussed without the limitations of experimental equipment and could be potentially helpful in future experiment designs and verifications.

In this work, by cascading the effects of SHG and THG, the resulting high harmonic and quasi-supercontinuum (quasi-SC) generations by ENZ AZO nanolayers are investigated numerically. Owing to the high second- and third-order susceptibilities of the AZO, a 100-nm thick ENZ AZO nanolayer can generate high harmonic waves up to the 15th order, with a pump source of a 1-ps or a 100-fs laser at telecommunication wavelength. Particularly, the spectral conversion efficiencies for the third- ($\sim 2.8\times 10^{-4}$), fifth- ($\sim 2.8\times 10^{-7}$) and seventh-harmonic generations ($\sim 2.4\times 10^{-8}$), estimated by the ratio of the spectral peak power, are in theory, comparable with the experimental results of ENZ indium tin oxide (ITO, THG $\sim 3.3\times 10^{-6}$) [18] and indium-doped cadmium oxide (ICO, $\sim 10^{-5}$, $\sim 10^{-8}$, and $\sim 10^{-10}$) [19]. In addition, the quasi-SC spectra produced in nanolayers with different thicknesses by ultrashort 10-fs pump source are discussed. The results of this work might be potentially useful in designing nanoscale multiwavelength light sources and frequency conversion devices.

* Corresponding author.
E-mail address: liqian@pkusz.edu.cn (Q. Li).

https://doi.org/10.1016/j.rinp.2021.104086
Received 9 December 2020; Received in revised form 12 March 2021; Accepted 14 March 2021
Available online 27 March 2021
2211-3797/© 2021 The Author(s). Published by Elsevier B.V. This is an open access article under the CC BY license (http://creativecommons.org/licenses/by/4.0/).

The paper is structured as follows. Firstly, the model and theory for cascaded HHG are introduced. Then the HHGs in ENZ AZO nanolayers excited by pump sources with different pulse durations are analysed. Subsequently, discussions on the quasi-SC generation by ENZ AZO nanolayers with different thickness is presented. Finally, the conclusions of this paper are drawn.

Model and theory

The ENZ AZO material can be fabricated by the state-of-the-art magnetron sputtering, chemical vapor deposition, and atomic layer deposition techniques [1,3]. To precisely illustrate the complex permittivity of the AZO, the well-received Drude model [3,27] is used, and it describes the relation between the complex permittivity ε, and the real and imaginary parts, ε_r and ε_i as:

$$\varepsilon = \varepsilon_r + i\varepsilon_i = \varepsilon_b - \frac{\omega_p^2}{(\omega^2+\gamma^2)} + i\frac{\omega_p^2\gamma}{(\omega^2+\gamma^2)\omega}, \tag{1}$$

where the high-frequency permittivity ε_b is 3.8, ω is the angular frequency of the EM wave, $\omega_p = 2.37\times10^{15}$ rad/s is the plasma frequency, and $\gamma = 6.80\times10^{13}$ rad/s is the Drude damping rate [1]. By adjusting the dopant concentration, the ENZ wavelength where ε_r reaches zero is tuned exactly at the telecommunication wavelength of 1550 nm, as shown in Fig. 1(a).

For TCOs like ENZ AZO, the heavy dopant concentration leads to structure degradation [28], defects such as oxygen vacancies are formed which will decrease the second-order susceptibility $\chi^{(2)}$ present in the bulk. However, the SHG and sum-frequency generation (SFG) [29] effects of $\chi^{(2)}$ can be observed near the surface in ITO [15,16,30] and AZO [31] due to the symmetry breaking at the surface [32,33,16,34]. Here, to incorporate the second-order nonlinearity into the simulation, we use the calibrated experimental value from the surface $\chi^{(2)}$ via Bloembergen-

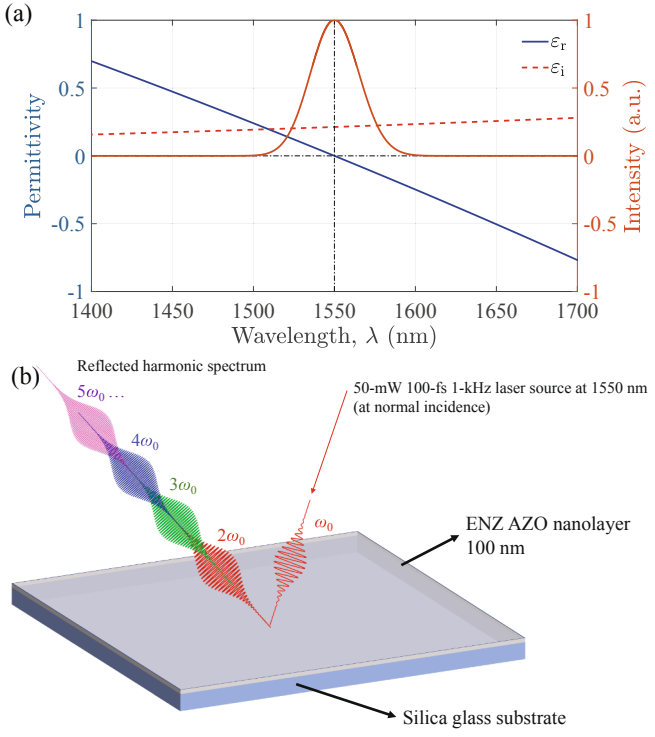

Fig. 1. (a) The complex permittivity of ENZ AZO nanolayer versus the spectrum of the 100-fs pulse. (b) The schematic diagram of an ENZ AZO nanolayer deposited on a silica glass substrate, producing HHG in its reflection spectrum. The colors of the HHG only represent the different frequencies of the EM waves, not their actual colors in the visible spectrum.

Pershan correction [35] of $\chi^{(2)} = 9.93\times10^{-13}$ m/V [31] for AZO. The third-order susceptibility $\chi^{(3)}$ which is responsible for THG, four-wave-mixing, and Kerr response [29], is 4.62×10^{-22} m^2/V^2 [31] near the telecommunication wavelength. The HHGs are caused by the higher orders of susceptibilities and modeled by the non-perturbative theory [36], which involves light-matter interactions in the quantum mechanical regime and ultrahigh input intensity with decreasing efficiencies. Instead, cascaded HHGs can be achieved by accumulating the effects of SHG, THG, and SFG [37] in both waveguides [38,39], crystals [39,40], and bulk plasmonic materials [41], extending from near-infrared (NIR) to extreme UV [38]. This scheme is suitable for ENZ TCO subwavelength materials due to their rich light-matter interactions, multiple EM energy reflections and localizations [13,14]. The energy of the generated harmonic EM waves can be redistributed to higher orders by yielding their own harmonic waves besides the base frequency. The behaviors of the EM wave under the subwavelength setups of this article can be described by the nonlinear Maxwell's equations [29]:

$$\begin{aligned}
&\nabla\times\mathbf{H} = \frac{\partial\mathbf{D}}{\partial t}, \nabla\times\mathbf{E} = -\frac{\partial\mathbf{B}}{\partial t},\\
&\mathbf{D} = \varepsilon_0\varepsilon\mathbf{E} + \mathbf{P}_{NL},\\
&\mathbf{P}_{NL} = \varepsilon_0\left(\chi^{(2)}:\mathbf{EE} + \chi^{(3)}\vdots\mathbf{EEE}\right),\\
&\mathbf{B} = \mu_0\mathbf{H}.
\end{aligned} \tag{2}$$

where $\mathbf{E}$ and $\mathbf{H}$ are electric and magnetic fields, $\mathbf{D}$ and $\mathbf{B}$ are electric and magnetic inductions, $\mathbf{P}_{NL}$ is the nonlinear electric polarization, and it is closely related to the second- and third-order susceptibilities $\chi^{(2)}$ and $\chi^{(3)}$ as shown in Eq. (2). The vacuum permittivity $\varepsilon_0 = 8.85\times10^{-12}$ F/m and the vacuum permeability $\mu_0 = 4\pi\times10^{-7}$ N/A^2. It would be difficult to manually solve Eq. (2) by hand, and in this work, the nonlinear Maxwell's equations are numerically solved by the finite-difference time-domain (FDTD) method using the commercially available software by Lumerical. The simulations in this work are performed with the Raman effects neglected.

HHGs in ENZ AZO nanolayers

To excite HHGs in ENZ AZO materials, a proper pump source should be used. In ENZ SHG, THG, and HHG experiments, milliwatt-grade low repetition rate femtosecond sources by the state-of-the-art solid-state lasers are often used [15,18,19], in order to acquire a relatively high peak power for a single pulse. In this study, a 50-mW, 1-kHz repetition rate, 100-fs laser source at 1550 nm is used, whose values are considered based on previous experimental studies (e.g. Ref. [19]). These specifications can be satisfied by using a tunable titanium-sapphire solid-state laser. Also in experiments, 20 nm to near 100 nm thick samples are often used [19,16], therefore, a thickness of 100 nm is chosen for the ENZ AZO nanolayer. Fig. 1(b) shows a schematic diagram of the ENZ AZO nanolayer deposited on a silica glass substrate, and the HHG produced in the reflection spectrum.

Chirp-free Gaussian pulses with a full width at half maximum intensity (FWHM) of 100 fs are assumed as the incident pulses, whose spectrum is shown in Fig. 1(a). To estimate the peak power and electric field amplitude of a single pulse, we assume a focus spot of 10 μm in diameter, which will give an average intensity of 6.37×10^4 W/cm^2. With an FWHM of 100 fs and a repetition rate of 1 kHz, this intensity is sufficiently high to drive HHGs and SFG in ENZ AZO nanolayers. In order to have a fair comparison, the peak intensity is held equal in our study here for both picosecond and femtosecond pump pulses. The pulses are injected onto the ENZ AZO nanolayer at normal incidence, and the data are collected from the reflected waves, as shown in Fig. 2.

As can be seen from Figs. 2(a) and 2(b), the 100-nm thick ENZ AZO nanolayer can yield HHG up to the 15th order by the 1 ps and 100 fs sources. Due to the wider bandwidth of the 100-fs source, other frequency components in the proximity of the central wavelength 1550 nm

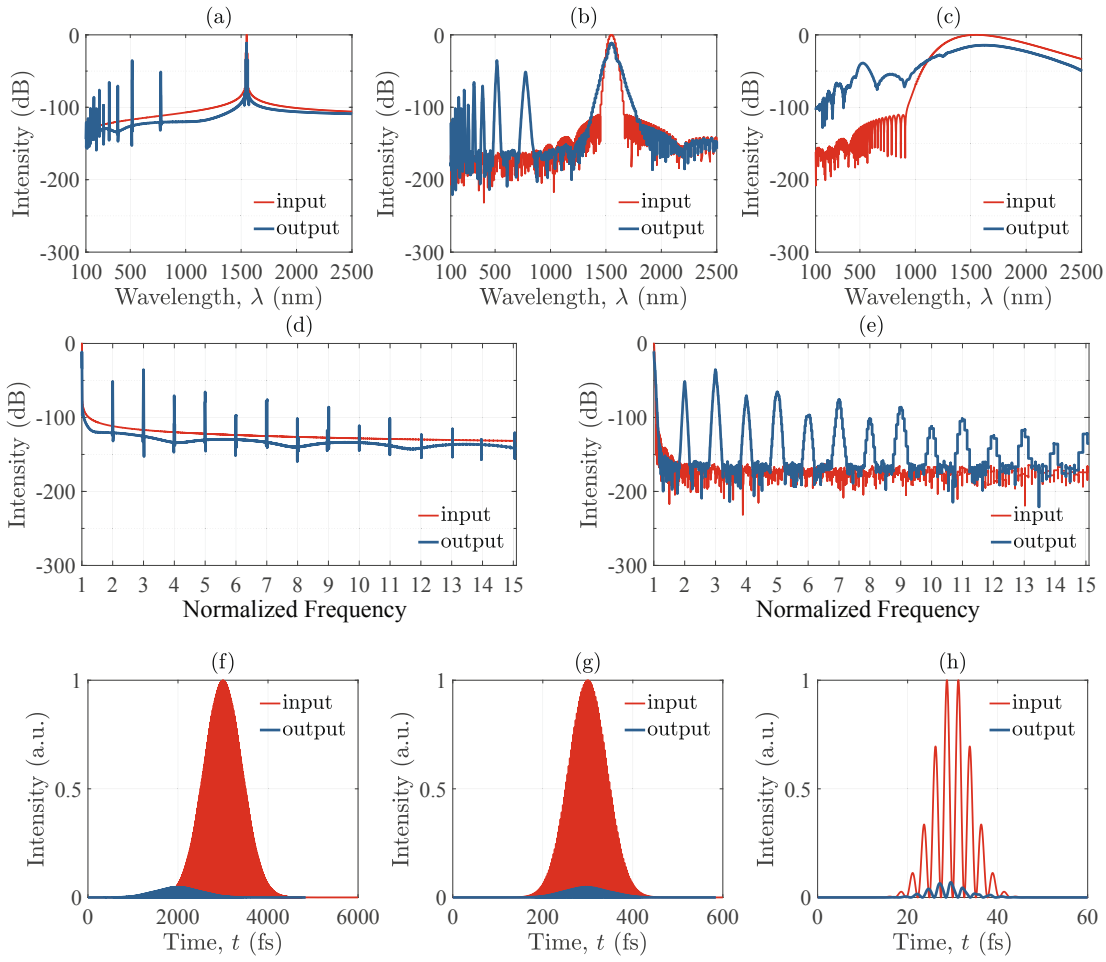

Fig. 2. HHG spectra by ENZ AZO nanolayers with (a) 1 ps, (b) 100 fs, and (c) 10 fs pump source. (d) and (e) are the normalized frequency view of the short-wavelength regions in (a) and (b) in the form of the multiples of the original (base) frequency of 1550 nm. The temporal shapes of the input and output pulses of (f) 1 ps, (g) 100 fs, (h) 10 fs.

also involve in HHG and SFG, causing wider high-harmonic peaks in Figs. 2(b) and 2(e) compared with Figs. 2(a) and 2(d). The short-wavelength regions of the spectra in Figs. 2(a) and 2(b) are very crowded, and to clearly show the order of the harmonic waves, in Figs. 2(d) and 2(e) we expand these two subfigures in the form of the multiples of the original (base) frequency at 1550 nm. Therefore, all orders of HHGs are equally separated and can be labeled with integers. One can see that the 2nd to the 15th harmonic generations cover a large section of the spectrum, from NIR all across the visible spectrum to the UV regime. In the simulation, orders higher than the 15th are of very low efficiencies and almost non-distinguishable from the background. Here, the simulated HHG results and the nanoscale of the structure indicate that the ENZ AZO nanolayers might be useful in designing integrated multi-wavelength light sources and frequency conversion devices.

In order to estimate the energy conversion efficiencies of the HHGs, we define the spectral conversion efficiency (SCE) as the ratio between the peak intensity of the harmonic wave and the incident wave. This method is comparable with those used in experiments, and it is found that, for the 1-ps and 100-fs sources, the SCEs for the third- ($\sim 2.8 \times 10^{-4}$), fifth- ($\sim 2.8 \times 10^{-7}$) and seventh-harmonic generations ($\sim 2.4 \times 10^{-8}$), are in theory, comparable with the experimental results of ENZ ITO (THG, $\sim 3.3 \times 10^{-6}$) [18] and ICO ($\sim 10^{-5}, \sim 10^{-8}$, and $\sim 10^{-10}$) [19]. However, in reality, the samples are not perfectly defect-free as in theoretical models. It is already known that the fabrication methods, the annealing conditions, the storage environment, and after-treatments can all affect the physical parameters such as the damping rate, the permittivity, and the susceptibility, leading to a very different SCE. Therefore, the purpose of the comparison here is to give a general idea of the strength of HHG in ENZ AZO nanolayers.

It is worth noting that, due to a much broader spectrum induced by the 10-fs source and the interactions of different frequencies, the HHGs in Fig. 2(c) are not distinguishable from each other. They tend to connect and form a quasi-SC spectrum. This is quite different from the cases with the 1-ps and 100-fs sources in Figs. 2(a) and 2(b), and will be discussed separately in the next Section. In Figs. 2(f)–2(h), the temporal peak intensity of the output pulses is significantly lower than the input pulse. The temporal energy is only $\sim$ 3.63% of the initial pulse, indicating a relatively large linear loss.

Discussions on quasi-SC generations

As mentioned in Fig. 2(c), the 100-nm thick ENZ AZO nanolayer can generate a quasi-SC spectrum by a 10-fs laser source due to the broad bandwidth of each harmonic peaks. The definition of a quasi-SC spectrum in previous works is that the original pulse is altered so rapidly and continuously that it looks like an SC spectrum [42]. In Fig. 2(c) the cascaded HHG peaks are so continuously connected that it seems as if the main pulse expands itself into the visible and the UV regime. Therefore, we also call it a cascaded-harmonic-induced quasi-SC spectrum. This kind of quasi-SC is different from conventional SC because the latter is basically the broadening of the original pulse spectrum around its central wavelength [43].

In experiments, due to the nature of the deposition and annealing

processes, the physical properties such as structural stress, permittivity, and susceptibility, can be not strictly isotropic and even be anisotropic. It is found that the nonlinear effects can be boosted at oblique incidence [44,12]. However, due to the limitations in simulations, TCO nanolayers are treated as near-isotropic materials. With this condition, involving oblique incidence under nonlinear setups can lead to results far from the experiment observations, and there is only one free dimension left to discuss: the thickness. Due to the existence of the non-negligible nonlocal effects in ultrathin films [45], the ENZ effect might even be diminished and their behaviors can be very different, we only consider thicknesses greater than 50 nm. In Fig. 3, comparisons of the quasi-SC spectra by different thicknesses of ENZ AZO nanolayer are presented. Fig. 3(a) shows the spectrum of the input pulse versus the output spectra of the 50-nm, 100-nm, 200-nm, and 300-nm thick ENZ AZO nanolayers. Fig. 3(b) is the expanded view of Fig. 3(a).

From Fig. 3(a), it can be seen that the existence of the ENZ AZO nanolayer significantly lifts the intensity of the short-wavelength region ($\lambda < 1000$ nm) compared to the input pulse, and the HHG peaks are all non-distinguishable from each other. From Fig. 3(b), there exists a tendency that, the thicker the ENZ AZO nanolayer is, the flatter, smoother, and more continuous the quasi-SC spectra would be. Additionally, in Fig. 3(a) the 200-nm nanolayer yields a significantly higher SCE in the short-wavelength region than the 100-nm, for example, the intensity of the hump near $\lambda = 500$ nm of the 200-nm sample is around three orders of magnitude larger than the 100-nm sample. However, the improvement of the 300-nm sample is only less than 1 order of magnitude over the 200-nm one. The dip in the spectrum around 1400 nm in Figs. 3(a) and 3(b) would become deeper as the thickness increases, damaging the continuity of the quasi-SC spectrum. Therefore, under the setup of this study, an ENZ AZO nanolayer with a thickness of around 200 nm is better at generating a quasi-SC spectrum. Conventional SC generation often requires a large or long structure, for example, a segment of nonlinear fiber. The viability of the ENZ AZO nanolayer to generate quasi-SC indicates that it has the potential to be used in the designs of a compact nanoscale multiwavelength light sources.

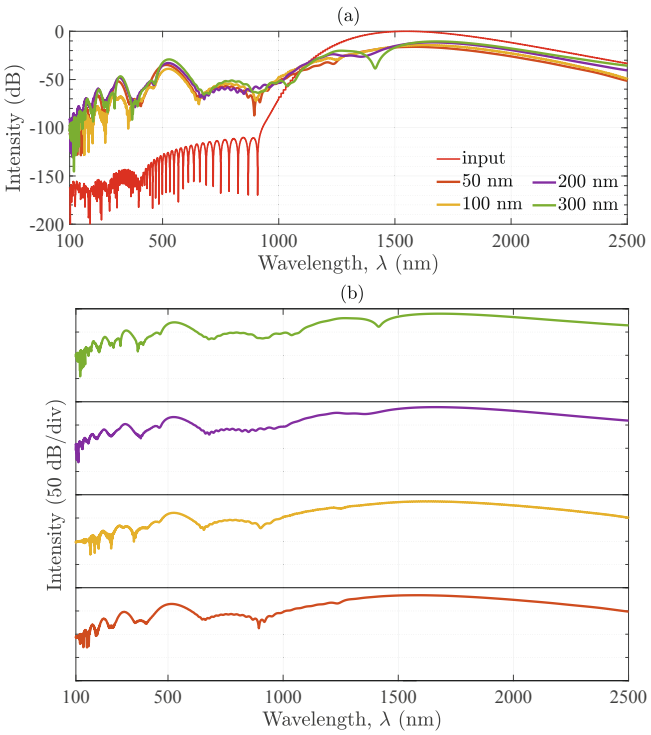

Fig. 3. Comparisons of the quasi-SC spectra of (a) input, 50-nm, 100-nm, 200-nm, and 300-nm thick ENZ AZO nanolayers, and (b) is the expanded view of (a).

Conclusions

In this study, the cascaded HHGs and quasi-SC spectrum generations by ENZ AZO nanolayers are investigated numerically. Due to the high nonlinearity of the AZO, a 100-nm thick ENZ AZO nanolayer can have HHGs up to the 15th order pumped by a 1-ps or a 100-fs laser source at 1550 nm. Especially, the SCEs for the third- ($\sim 2.8 \times 10^{-4}$), fifth- ($\sim 2.8 \times 10^{-7}$) and seventh-harmonic generations ($\sim 2.4 \times 10^{-8}$) are in theory, comparable with the experimental results of ENZ ITO (THG $\sim 3.3 \times 10^{-6}$) and ICO ($\sim 10^{-5}$, $\sim 10^{-8}$, and $\sim 10^{-10}$).

Additionally, the quasi-SC spectra produced in nanolayers with different thicknesses by ultrashort 10-fs pump source are discussed, and it is found that under the settings of this study, a 200-nm thick ENZ AZO nanolayer yields smooth and continuous quasi-SC spectrum. The results of this work might be potentially useful in designing nanoscale multi-wavelength light sources and frequency conversion devices thanks to ENZ AZO's high nonlinearity, HHGs, quasi-SC generation capability, and CMOS-compatibility.

CRediT authorship contribution statement

Jiaye Wu: Conceptualization, Methodology, Software, Writing - original draft. **Ze Tao Xie:** Software, Validation. **H.Y. Fu:** Software, Supervision, Resources. **Qian Li:** Supervision, Resources, Writing - review & editing, Project administration, Funding acquisition.

Declaration of Competing Interest

The authors declare that they have no known competing financial interests or personal relationships that could have appeared to influence the work reported in this paper.

Acknowledgments

This work is supported by the National Natural Science Foundation of China (61675008); Shenzhen Science and Technology Innovation Commission (GJHZ20184111850152 72, JCYJ20180507183815699); Youth Science and Technology Innovation Talent of Guangdong Province (2019TQ05X227).

References

[1] Naik GV, Shalaev VM, Boltasseva A. Alternative plasmonic materials: beyond gold and silver. Adv Mater 2013;25:3264–94. https://doi.org/10.1002/adma.201205076.
[2] Liberal I, Engheta N. Near-zero refractive index photonics. Nat Photonics 2017;11:149–58. https://doi.org/10.1038/nphoton.2017.13.
[3] Niu X, Hu X, Chu S, Gong Q. Epsilon-near-zero photonics: a new platform for integrated devices. Adv Opt Mater 2018;6:1701292. https://doi.org/10.1002/adom.201701292.
[4] Kinsey N, DeVault C, Boltasseva A, Shalaev VM. Near-zero-index materials for photonics. Nature Rev Mater 2019;4:742–60. https://doi.org/10.1038/s41578-019-0133-0.
[5] Reshef O, De Leon I, Alam MZ, Boyd RW. Nonlinear optical effects in epsilon-near-zero media. Nature Rev Mater 2019;4:535–51. https://doi.org/10.1038/s41578-019-0120-5.
[6] Silveirinha M, Engheta N. Tunneling of electromagnetic energy through subwavelength channels and bends using ϵ)near-zero materials. Phys Rev Lett 2006;97:157403. https://doi.org/10.1103/PhysRevLett.97.157403.
[7] Enoch S, Tayeb G, Sabouroux P, Guérin N, Vincent P. A metamaterial for directive emission. Phys Rev Lett 2002;89:213902. https://doi.org/10.1103/PhysRevLett.89.213902.
[8] Campione S, de Ceglia D, Vincenti MA, Scalora M, Capolino F. Electric field enhancement in ϵ)near-zero slabs under TM-polarized oblique incidence. Phys Rev B 2013;87:035120. https://doi.org/10.1103/PhysRevB.87.035120.
[9] Vassant S, Hugonin J-P, Marquier F, Greffet J-J. Berreman mode and epsilon near zero mode. Opt Express 2012;20:23971. https://doi.org/10.1364/OE.20.023971.
[10] Ciattoni A, Marini A, Rizza C, Scalora M, Biancalana F. Polariton excitation in epsilon-near-zero slabs: transient trapping of slow light. Phys Rev A 2013;87:053853. https://doi.org/10.1103/PhysRevA.87.053853.

[11] Ciattoni A, Rizza C, Marini A, Falco AD, Faccio D, Scalora M. Enhanced nonlinear effects in pulse propagation through epsilon-near-zero media. Laser Photonics Rev 2016;10:517–25. https://doi.org/10.1002/lpor.201500326.
[12] Alam MZ, De Leon I, Boyd RW. Large optical nonlinearity of indium tin oxide in its epsilon-near-zero region. Science 2016;352:795–7. https://doi.org/10.1126/science.aae0330.
[13] Wu J, Malomed BA, Fu HY, Li Q. Self-interaction of ultrashort pulses in an epsilon-near-zero nonlinear material at the telecom wavelength. Opt Express 2019;27:37298–306. https://doi.org/10.1364/OE.27.037298. arXiv:1911.11917.
[14] Wu J, Xie ZT, Sha Y, Fu HY, Li Q. Comparative study on epsilon-near-zero transparent conducting oxides: High-order chromatic dispersions and modeling of ultrashort pulse interactions. Phys Rev A 2020;102:053503. https://doi.org/10.1103/PhysRevA.102.053503.
[15] Capretti A, Wang Y, Engheta N, Dal Negro L. Comparative study of second-harmonic generation from epsilon-near-zero indium tin oxide and titanium nitride nanolayers excited in the near-infrared spectral range. ACS Photonics 2015;2:1584–91. https://doi.org/10.1021/acsphotonics.5b00355.
[16] Rodríguez-Suné L, Scalora M, Johnson AS, Cojocaru C, Akozbek N, Coppens ZJ, Perez-Salinas D, Wall S, Trull J. Study of second and third harmonic generation from an indium tin oxide nanolayer: Influence of nonlocal effects and hot electrons. APL Photonics 2020;5:010801. https://doi.org/10.1063/1.5129627.
[17] Capretti A, Wang Y, Engheta N, Dal Negro L. Enhanced third-harmonic generation in Si-compatible epsilon-near-zero indium tin oxide nanolayers. Opt Lett 2015;40:1500. https://doi.org/10.1364/OL.40.001500.
[18] Luk TS, de Ceglia D, Liu S, Keeler GA, Prasankumar RP, Vincenti MA, Scalora M, Sinclair MB, Campione S. Enhanced third harmonic generation from the epsilon-near-zero modes of ultrathin films. Appl Phys Lett 2015;106:151103. https://doi.org/10.1063/1.4917457.
[19] Yang Y, Lu J, Manjavacas A, Luk TS, Liu H, Kelley K, Maria J-P, Runnerstrom EL, Sinclair MB, Ghimire S, Brener I. High-harmonic generation from an epsilon-near-zero material. Nat Phys 2019;15:1022–6. https://doi.org/10.1038/s41567-019-0584-7. arXiv:1902.03539.
[20] Tian W, Liang F, Lu D, Yu H, Zhang H. Highly efficient ultraviolet high-harmonic generation from epsilon-near-zero indium tin oxide films. Photonics Res 2021;9:317–23. https://doi.org/10.1364/PRJ.414570.
[21] Kinsey N, DeVault C, Kim J, Ferrera M, Shalaev VM, Boltasseva A. Epsilon-near-zero Al-doped ZnO for ultrafast switching at telecom wavelengths. Optica 2015;2:616. https://doi.org/10.1364/OPTICA.2.000616.
[22] Guo Q, Cui Y, Yao Y, Ye Y, Yang Y, Liu X, Zhang S, Liu X, Qiu J, Hosono H. A solution-processed ultrafast optical switch based on a nanostructured epsilon-near-zero medium. Adv Mater 2017;29:1700754. https://doi.org/10.1002/adma.201700754.
[23] Xie ZT, Wu J, Fu HY, Li Q. Tunable Electro- and All-optical Switch Based on Epsilon-near-zero Metasurface. IEEE Photonics J 2020;12:1–10. https://doi.org/10.1109/JPHOT.2020.3010284.
[24] Bellini M, Lyngå C, Tozzi A, Gaarde MB, Hänsch TW, L'Huillier A, Wahlström C-G. Temporal Coherence of Ultrashort High-Order Harmonic Pulses. Phys Rev Lett 1998;81:297–300. https://doi.org/10.1103/PhysRevLett.81.297.
[25] Hemsing E, Dunning M, Hast C, Raubenheimer TO, Weathersby S, Xiang D. Highly coherent vacuum ultraviolet radiation at the 15th harmonic with echo-enabled harmonic generation technique. Phys Rev Special Topics – Accel Beams 2014;17:070702. https://doi.org/10.1103/PhysRevSTAB.17.070702.
[26] Khurgin JB, Clerici M, Bruno V, Caspani L, DeVault C, Kim J, Shaltout A, Boltasseva A, Shalaev VM, Ferrera M, Faccio D, Kinsey N. Adiabatic frequency shifting in epsilon-near-zero materials: the role of group velocity. Optica 2020;7:226. https://doi.org/10.1364/OPTICA.374788.
[27] Drude P. Zur Elektronentheorie der Metalle. Ann Phys 1900;306:566–613. https://doi.org/10.1002/andp.19003060312.
[28] Kim J, Naik GV, Gavrilenko AV, Dondapati K, Gavrilenko VI, Prokes SM, Glembocki OJ, Shalaev VM, Boltasseva A. Optical Properties of Gallium-Doped Zinc Oxide–A Low-Loss Plasmonic Material: First-Principles Theory and Experiment. Phys Rev X 2013;3:041037. https://doi.org/10.1103/PhysRevX.3.041037.
[29] Agrawal GP. Nonlinear Fiber Optics. 5 ed. Academic; 2013.
[30] Deng J, Tang Y, Chen S, Li K, Zayats AV, Li G. Giant Enhancement of Second-Order Nonlinearity of Epsilon-near- Zero Medium by a Plasmonic Metasurface. Nano Lett 2020;20:5421–7. https://doi.org/10.1021/acs.nanolett.0c01810.
[31] Tian W, Liang F, Chi S, Li C, Yu H, Zhang H, Zhang H. Highly Efficient Super-Continuum Generation on an Epsilon-Near-Zero Surface. ACS Omega 2020;5:2458–64. https://doi.org/10.1021/acsomega.9b04026.
[32] Sipe JE, So VCY, Fukui M, Stegeman GI. Analysis of second-harmonic generation at metal surfaces. Phys Rev B 1980;21:4389–402. https://doi.org/10.1103/PhysRevB.21.4389.
[33] Scalora M, Vincenti MA, de Ceglia D, Roppo V, Centini M, Akozbek N, Bloemer MJ. Second- and third-harmonic generation in metal-based structures. Phys Rev A 2010;82:043828. https://doi.org/10.1103/PhysRevA.82.043828.
[34] Scalora M, Trull J, de Ceglia D, Vincenti MA, Akozbek N, Coppens Z, Rodríguez-Suné L, Cojocaru C. Electrodynamics of conductive oxides: Intensity-dependent anisotropy, reconstruction of the effective dielectric constant, and harmonic generation. Phys Rev A 2020;101:053828. https://doi.org/10.1103/PhysRevA.101.053828.
[35] Bloembergen N, Pershan PS. Light Waves at the Boundary of Nonlinear Media. Phys. Rev. 1962;128:606–22. https://doi.org/10.1103/PhysRev.128.606.
[36] Xu H. Non-perturbative theory of harmonic generation under a high-intensity laser field. Zeitschrift für Physik D Atoms, Molecules and Clusters 1993;28:27–36. https://doi.org/10.1007/BF01437452.
[37] Landry GD, Maldonado TA. Second-harmonic generation and cascaded second-order processes in a counterpropagating quasi-phase-matched device. Appl Opt 1998;37:7809. https://doi.org/10.1364/AO.37.007809.
[38] Comby A, Descamps D, Beauvarlet S, Gonzalez A, Guichard F, Petit S, Zaouter Y, Mairesse Y. Cascaded harmonic generation from a fiber laser: a milliwatt XUV source. Opt Express 2019;27:20383. https://doi.org/10.1364/OE.27.020383.
[39] Lu J, Liu X, Bruch AW, Zhang L, Wang J, Yan J, Tang HX. Ultraviolet to mid-infrared supercontinuum generation in single-crystalline aluminum nitride waveguides. Opt Lett 2020;45:4499. https://doi.org/10.1364/OL.398257.
[40] Ivanov R, Saltiel S. Cascaded fourth-harmonic generation in a single nonlinear crystal. J Opt Soc Am B 2005;22:1691. https://doi.org/10.1364/JOSAB.22.001691.
[41] Celebrano M, Locatelli A, Ghirardini L, Pellegrini G, Biagioni P, Zilli A, Wu X, Grossmann S, Carletti L, De Angelis C, Duò L, Hecht B, Finazzi M. Evidence of Cascaded Third-Harmonic Generation in Noncentrosymmetric Gold Nanoantennas. Nano Lett 2019;19:7013–20. https://doi.org/10.1021/acs.nanolett.9b02427.
[42] Sumimura K, Genda Y, Ohta T, Itoh K, Nishizawa N. Quasi-supercontinuum generation using 106μm ultrashort-pulse laser system for ultrahigh-resolution optical-coherence tomography. Opt Lett 2010;35:3631. https://doi.org/10.1364/OL.35.003631.
[43] Li G, Li Q. Picosecond pulse pumped supercontinuum generation in silicon waveguide with a weak continuous wave trigger. J Opt Soc Am B 2020;37:1749. https://doi.org/10.1364/JOSAB.390825.
[44] Vincenti MA, de Ceglia D, Ciattoni A, Scalora M. Singularity-driven second- and third-harmonic generation at ϵ)near-zero crossing points. Phys Rev A 2011;84:063826. https://doi.org/10.1103/PhysRevA.84.063826.
[45] Zheng H, Zhang R-J, Li D-H, Chen X, Wang S-Y, Zheng Y-X, Li M-J, Hu Z-G, Dai N, Chen L-Y. Optical Properties of Al-Doped ZnO Films in the Infrared Region and Their Absorption Applications. Nanoscale Res Lett 2018;13:149. https://doi.org/10.1186/s11671-018-2563-9.